Chapter 3: EUV/FUV High-Throughput Spectroscopic Telescope

3.1. Performance requirements for the spectrometer

The Solar-C mission provides an ideal platform for a EUV/FUV high-throughput high-resolution spectrometer (may be called EUVS hereafter). Performance requirements are summarized below for a breakthrough spectroscopic instrument, which can be realized with recent technology advancements.

1. *To operate in both spectroscopic and imaging modes with high temporal resolution (cadence).* This is required for quantitatively understanding the physics of dynamical phenomena. One order of improvement in effective area is required. Thus, the temporal resolution at a slit position can be shortened down to 0.5 sec for active region plasma and 1 sec for quiet Sun plasma.
2. *To perform EUV/FUV spectroscopy with high spatial resolution.* The spectrometer is required to resolve structures equal to 0.5" resolution or better. The target is 0.3 arcsec, which is roughly equivalent to the width of chromospheric spicules observed with Hinode/SOT.
3. *To observe a field of view as large as possible.* The best resolution may be restricted to ~5x5 arcmin^2 (a medium size active region), but lower resolution should cover a larger field of view.
4. *To perform EUV/FUV spectroscopy with high spectral resolution.* The spectrometer is required to determine Doppler velocities to an accuracy of ~ 2 km/s from spectral line shifts and non-thermal motions as small as 20 km/s from line widths.
5. *To make measurements with spectral lines from a broad temperature range and with adequate plasma diagnostics covering chromospheric, transition region, low corona and flare temperatures.* The observations must cover all relevant temperatures and structures in order to track the flow of energy from the chromosphere into the corona.
6. *To perform good observations with low-scattering optics.* This performance is needed to explore "faint" reconnection outflow regions, coronal holes, and off-limb observations.
7. *To ensure precise co-alignment with the data from other onboard telescopes.* Co-alignment must meet the high spatial resolution of the spectrometer.

The performance requirements summarized above are determined from the science goals in section 1. Table 3.1 summaries instrument performance required for the Solar-C spectrometer, compared with the previous spectrometers. It is obvious that the Solar-C spectrometer will have significant improvements on the temporal resolution, spatial resolution, and temperature coverage. Some of the performance required for the Solar-C spectrometer are discussed below to show possible discovery spaces and new sciences.

Table 3.1. Performance of Solar-C spectrometer in comparison with other spectrometers

	Solar-C spectrometer	Hinode/EIS	SoHO/SUMER
Temporal resolution for a slit position *1	0.5 - 10 sec for AR 1 -10 sec for QS	10 - 20 sec for AR 30 – 60 sec for QS	10 – 20 sec for AR line *2
Spatial resolution	~0.3 arcsec (target) ~0.16 arcsec (pixel size)	3-4 arcsec 1arcsec (pixel size)	2 arcsec 1arcsec (pixel size)
Primary temperature coverage ($\log_{10}$ K)	4.1 – 7.2	4.9, 5.6-7.2	4.1-5.8

*1 The values given here are typical exposure duration for multiple numbers of spectral lines covering a wide temperature range.

*2 SUMER can record spectral lines in only one of spectral windows at the same time. If spectral lines in another spectral window are measured, the grating is needed to move before the exposure.

3.1.1. Spatial resolution requirement

One of key tasks of EUVS is to precisely measure plasma conditions, such as temperature, density, and velocity of elementary structures of the magnetized atmosphere in all temperature regions from the chromosphere through transition region and into the corona. Such measurements made simultaneously with different spectral lines allow us to trace the flow of energy from the chromosphere up into the corona. In the photosphere the energy is observed to be in plasma structures with a scale length of about 0.3″ or about 200 km. Movies made in the Ca II H-line from Hinode SOT clearly reveal that the chromosphere is dominated by a multitude of thin (~200 km), dynamical, jet-like extrusions called spicules. Since SOT can carry out only imaging observations for the chromosphere without spectroscopic capabilities, the proposed spectrometer will be the first instrument to diagnose the plasma properties of these thin, dynamical structures and to follow these structures upwards through the atmosphere into the corona. As the magnetic field may expand with height, the overall size of structures may increase as they rise above the chromosphere/transition region, but the width of spicules may be preserved into the transition region and corona. Coronal loops are well-known coronal magnetic structures, but elementary structures are not yet fully resolved in the corona with the currently existing imaging telescopes (0.″5 at the highest resolution). Spectroscopic measurements in the EUV have suggested that only 10% of the volume of coronal loops is filled with hot plasma, when they are observed with the spatial resolution of 2-3 arcsec (pixel size 1 arcsec) (Warren et al. 2008). Thus, measuring the plasma parameters with 0.3 arcsec, i.e., 10% of the 1 arcsec volume, can fully resolve elementary structures hidden in the magnetic loops. Understanding the magnetic sub-structure implied by the small filling factor is crucial for determining energy flow in coronal loops and ultimately for understanding the physics of coronal heating.

In addition to its own scientific contribution, the spectrometer observations shall have close scientific synergy with the other proposed telescopes. One of the important science goals is to understand the roles of waves propagating through the atmosphere in heating and activating dynamical motions in the plasma. It is important to determine whether or not sufficient energy remains in the waves that penetrate all the way to the corona to make a substantial contribution to the heating budget of the solar corona and/or to the acceleration of the solar wind. It is also critical to identify propagating MHD waves and their modes. For this purpose, observations of magnetic field fluctuations are required in addition to observations of intensity and velocity fluctuations. The proposed spectrometer can provide the observation of intensity and velocity fluctuations. Magnetic field measurements are available only for the low atmosphere, i.e., in the photosphere and chromosphere, and they will be provided by the

UV-Visible-IR telescope with a spatial resolution of 0.2″ or better. The UV-Visible-IR telescope is designed to determine the modes and amplitudes of waves in the low atmosphere just after the excitation of the waves, and the proposed spectrometer can continue to trace their propagation into the transition region and corona. With these coordinated observations, we will explore for the first time the mode conversion in waves, which is expected in the atmospheric layer where the plasma beta is unity. Since the plasma beta changes from high ($\beta>1$) in photosphere and low chromosphere to low ($\beta << 1$) in the corona, we can observe how the waves are evolved as a function of height in the stratified atmosphere. With having high spatial resolution never achieved so far, we can newly explore behaviors of waves and turbulence in small scale, which are useful information for physically understanding roles of waves in the atmosphere. We may have new information concerning turbulent cascade and phase mixing of Alfvenic waves.

Considering these new discovery spaces, the proposed spectrometer should have the capability of resolving structures with scales smaller than 350 km (0.5″). Ideally, it would be better to resolve even smaller structures, say, 0.3″ or ~200 km.

3.1.2. Temporal resolution requirement

Since the structures to be resolved with EUVS are small and dynamic, a high time cadence is necessary and consequently a high-throughput instrument is required. As a goal of the instrument design, the effective area of the spectrometer is set to be at least 10 times larger than previous instruments (EIS onboard Hinode, SUMER and CDS onboard SoHO). This means an improvement of at least an order of magnitude in temporal resolution if observing with the same sampling scale (~1″ arcsec). There is also an improvement even when observing with higher spatial resolution (0.5″ arcsec) than achieved with previous instruments. In the case of EIS observations, typical integration times of an exposure are 10 to 20 s for active region emission lines and 30-60 s for the quiet Sun (Note that shorter exposures are possible in very limited numbers of brighter lines). SUMER observations are carried out with 10 to 20 s integration times (shorter exposures would be possible in the brighter lines but the exposure time is limited by the available telemetry rate). With having high throughput performance and bright spectral lines, the integration times of the proposed spectrometer can be shortened down to 1-0.5 s. The sit-and-stare measurements at a slit position provide time series of spectral data with temporal resolution of 0.5-1 s. The field of view with 15 arcsec width can be repeatedly measured with 25-50 sec cadence, if the slit step is 0.3 arcsec. The spectral maps for 100 arcsec field of view are available every ~200 s, if the slit is stepped per 0.6 arcsec.

As discussed in section 1, numerical simulations suggest that low-frequency (<5mHz) magnetoacoustic waves may provide a significant source of the energy necessary for maintaining the chromosphere. Moreover, the outgoing low-frequency (<1mHz) Alfven waves may provide a major contribution to the heating and acceleration of the plasma as a result of the nonlinear generation of the compressive waves and shocks in the corona. Observationally, various kinds of oscillations and waves have been detected with Hinode data. For example, with analyzing EIS spectral data, upwardly propagating and standing slow magnetoacoustic waves are reported in active regions (Kitagawa et al. 2010) and coronal holes (Banerjee et al. 2009). When the waves propagates along a coronal loop with the sound speed (~150 km/s in the corona), the proposed spectrometer can scan the entire coronal loop about 5 times with 0.6 arcsec step during the time when the waves propagates from one end to the other end of the loop. Thus, such data will allow us to trace the waves from the excitation to the dissipation. The speed of Alfven waves is much higher than the sound speed in the

transition region and corona, but the scan speed of the proposed spectrometer can allow us to explore the properties of propagating Alfven waves, if we choose slit scan step size properly. Moreover, owing to higher temporal resolution, we will search for higher frequency waves (~1Hz) that cannot be explored with the currently existing spectrometers. If higher frequency waves are found in the transition region and corona with sufficient flux, high frequency waves may be a possible candidate for making the bright corona in active regions.

High temporal cadence performance with high spatial resolution has the potential to resolve fine dynamical structures in the coronal loops. Hinode EIS has revealed excess non-thermal line broadening at the footpoints of coronal loops, which is interpreted as the existence of highly blue-shifted small-scale flows at the base of coronal loops (Hara et al. 2008). Non-thermal line broadening is known in spectral lines from the transition region and corona, and we guess that the broadening is created by turbulent nature in coronal loops. Having short integration time is definitely useful to distinguish each of turbulent flows, providing new information on interpreting non-thermal line broadening.

Higher temporal cadence would provide strong tools in exploring coronal holes. Existing spectrometers need much longer integration times to meaningfully record spectral data in coronal holes, where the FUV and EUV coronal emissions are much fainter than in active regions. It is important to identify the source region of the fast solar wind in polar coronal holes. Because of very long integration times (several minutes for a slit position and several hours for mapping a region), it is difficult with existing instruments to confidently identify the source regions. A substantial improvement in the throughput performance can much reduce the time needed to spectrally map a region, getting closer to the timescales for the evolution of the structures. Also, waves with periods from 7 to 20 min have been detected in plumes and inter-plumes above the limb in the polar regions (DeForest & Gurman 1998; Ofman et al. 2000; Banerjee et al. 2000, 2009). A high throughout performance could allow a search for higher frequency waves in coronal holes and a search for wave signatures in line widths and velocity.

3.1.3. Broad temperature coverage

As one of the top-level science goals, we will attempt to understand how the energy is transported through elementary magnetic structures from the chromosphere to the transition region, and from the transition region into the corona. Furthermore, magnetic energy dissipation events are well observed over the entire solar atmosphere, not only in the outer corona which is filled with fully ionized, collisionless plasma, but also in the chromosphere which consists of weakly ionized plasma. In order to capture the entire picture observationally, it is important to measure the plasma conditions and behaviors in different temperature layers simultaneously.

SoHO/SUMER records spectral lines at longer wavelengths in the FUV, where many spectral lines originating from the transition region and chromosphere are available, while only few coronal lines are observed. In contrast, Hinode EIS observes spectral lines at shorter wavelength in the EUV, where many spectral lines from the corona and flare plasma are available but the number of spectral lines is limited for exploring the transition region and chromosphere. Extensive coordinated observations by the two instruments have been obtained since the launch of Hinode, providing significant new results. However, we realize that it is impossible to achieve high accuracy in the co-alignment of the spectral data from SUMER and EIS. Also, since the spectral data are acquired for a single slit position and it takes a long time to map a large field-of-view, it is nearly impossible for two different slit spectrographs to obtain data at the same location on the Sun and at the same time. However, observations at

the same locations and times are critical for understanding the dynamical behavior and evolution of the plasma in the observed targets, because the timescales for the evolution of structures are quite short.

Therefore, it is a requirement that the next generation advanced EUV/FUV spectrometer capture spectral data over the entire temperature domain of the solar atmosphere at the same locations and times. This performance can much improve and ensure accurate co-alignment among different spectral lines. With this improvement, we can discuss with high confidence the relationships among the observational signatures at different temperatures. Elementary magnetic structures of the order of 0.3″ seen in the chromosphere can then be traced into the transition region and corona. It is also possible to trace the flow of energy through static elementary magnetic structures over the solar atmosphere and quantitatively investigate the role of waves as a transporter of energy for heating the corona and energizing the solar wind.

3.1.4. Necessity of low scattering optics

Low-scattering optics should be considered when the spectrometer is designed and fabricated to allow us to accurately record low intensity data. A single-mirror, off-axis telescope is mandatory for off-limb observations, to avoid stray light from the bright solar disk. Many important science discoveries may be hidden in low emission measure areas such as reconnection outflow regions, which are much fainter than flare loops. As another example, low intensity emission in coronal holes observed off-limb may hold the key for understanding solar wind acceleration and shock formation in the high corona.

The reconnection region science discussed in section 1.3.4.2 is an excellent example for stressing the importance of low-scattering performance. Probing the reconnection region itself is not easy because intense flare loops are formed near the reconnection region due to chromospheric evaporation. According to the model calculation given in section 1.3.4.2, the total intensity of the reconnection outflow region is about one thousandths of the total intensity of the bright post-flare loops, when observed in spectral lines from Fe^{+17} to Fe^{+23}. This estimate tells us that low-scattering optics are necessary for investigating the flare reconnection outflow region.

3.1.5. Substantial jump expected from the NASA IRIS mission

IRIS (Interface Region Imaging Spectrograph) is a NASA SMEX mission selected for launch in December 2012. This spectrograph observes several spectral lines in the 120 to 280 nm range with high spatial resolution (0.3″) and high cadence (1 to 5 sec), to discover how the outer atmosphere is energized. The spectral lines observed with IRIS are suitable for exploring the interface between the upper chromosphere and lower transition region, and the IRIS mission is expected to open a window of discovery into a crucial gap in current solar observational capabilities.

However, the spectrometer proposed here would provide a substantial step forward from IRIS observations, because the Solar-C Plan B mission can provide unique observations that have never been realized, allowing us to progress beyond the chromosphere-transition region interface into the entire transition region and corona. The proposed spectrometer will be able to observe spectral lines in the EUV and FUV that seamlessly cover all the temperatures from the chromospheric to the corona with high spatial resolution (0.5″ or better) and high cadence (1 to 5 s). Observations of this completeness are necessary for understanding coronal heating and the formation of the solar wind. In addition, the proposed spectrometer observes several spectral lines that originate from high temperature plasma in the 10^6-10^7 K temperature range,

and these spectral lines are useful for diagnosing flares and active region dynamics in the corona. Thirdly, and more important, is that EUV and FUV spectroscopic observations can be carried out simultaneously with quantitative measurements of magnetic fields in the chromosphere and photosphere with 0.1″ to 0.2″, taken by the UV-Visible-IR telescope. This would be an enormous help in associating an accurate magnetic geometry with the EUV-FUV spectra. Finally, unlike IRIS, the single-mirror off-axis design of the telescope allows us to observe faint structures in the corona far from the solar disk.

3.2. Technical feasibility of each key element

The strawman instrumentation draws heavily on current technology under development by the international EUV/FUV spectroscopic community. Technical feasibility of each key technology is briefly described below.

3.2.1. Two element optical layout

In order to improve throughput performance, minimizing the number of optical elements is essential; the spectrograph consists of two optical elements, i.e., an off-axis parabola primary mirror and a concave grating. The two-element spectrograph design was first developed and flown for EIS onboard Hinode and it has since been refined to meet various requirements for RAISE, VERIS and EUNIS rocket payloads.

3.2.2. The telescope mirror and mirror coating

For off-limb solar observations the single-mirror telescope greatly reduces stray light, as compared to an on-axis, double-mirror design. In addition, a secondary mirror would not only reduce throughput by adding another reflection but would also be vulnerable to degradation due exposure to very high solar flux. Thus the decision is made for a single-mirror telescope.

Increasing the size of the primary mirror gives a significant improvement in throughput. If the diameter of the mirror can be increased twice, the effective area is improved by a factor 4. 30 cm or larger diameter gives 4 times or larger throughput, as compared with EIS (diameter 15cm).

Driven by requirements for EUV photolithography, EUV optics with very low scatter and diffraction limited performance are available. For example, the optics developed for the MET EUV photolithographic system have a slope error of 0.3 to 1.0 microradians, and microroughness of 0.1 to 0.2 nm over spatial frequencies from 9 nm to 4 mm (Goldberg et al. 2005).

A single coating on the primary mirror – without division in sections for EUV and FUV ranges - results in good performance across a broad wavelength range. The suggested coating is described in Figure 3.1. It consists of a broadband Si/Mo multilayer with a 5 nm B_4C topcoat. The B_4C topcoat is semi-transparent in the EUV but gives reasonable reflectance at longer wavelengths as shown in Figure 3.1 (left). The single coating minimizes risk and complexity for the primary mirror associated with dividing the solar illuminated mirror into segments with different coatings. Recent advances in stabilizing multilayer for higher temperature performance will be incorporated into the multilayer coating design.

3.2.3. Grating and grating coating

To realize seamless temperature coverage in the 10^4 to 10^7 K range, the spectrometer needs to cover between 2 and 4 wavelength bandpasses over a range from 10 nm to 120 nm. To accommodate this broad wavelength range, the grating is divided into two segments. The ruling density, groove geometry and figure of each segment is optimized for the specific wavelength range. Each grating segment is coated individually. A process is envisioned where each coated grating segment would be contacted/cemented to a common plate. This plate would then be installed into the instrument.

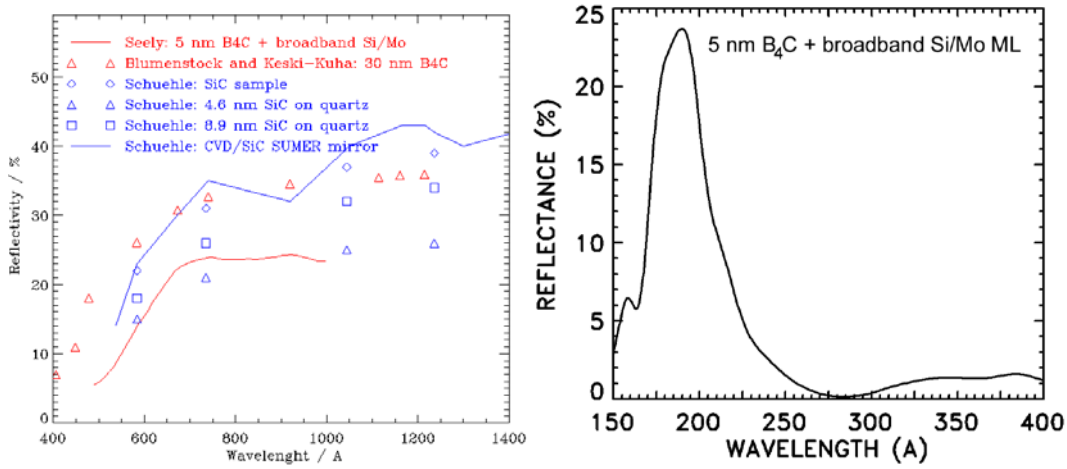

Figure 3.1. Reflectivity of the proposed primary mirror coating. The red curve in the left panel shows the performance of the coating from 50 to 120 nm. The right panel gives the EUV coating performance.

3.2.4. Solar blind detectors for EUVS

Enhanced technology detectors with larger format and faster readout are under development for space flight. The intensified (CMOS-APS) active pixel sensor (flown on NASA's EUNIS and RAISE rocket flights) has the promise of exceptionally fast image readout with quick access to specific pixel areas. The intensifier with opaque anode ensures that the detector is "solar blind" and focal plane filters, to suppress visible solar radiation, are not needed. The opaque photocathode on the microchannel plates will ensure very high sensitivity in selected spectral ranges.

At shorter wavelengths (in the EUV), back side thinned, large format, fast readout silicon based CCD and APS detectors are highly efficient, low-noise, fast-readout detectors. The backside illuminated detectors will be fitted with focal plane filters to provide rejection of the visible solar radiation scattered from the grating. The performance of currently available intensified CCD and EUV backside illuminated CCDs are suitable for the EUVS mission while similar CMOS-APS sensors are presently under development.

3.2.5. Removal of metal filters and thermal control concept

To achieve low scatter, higher throughput and broad wavelength coverage, the EUVS strawman design has no prefilters in the front aperture. These prefilters have historically been used to protect the multilayers from the incident solar radiation. With one solar constant illuminating the primary mirror, the temperature of the mirror is expected to increase to 50 °C

or 60 °C provided that a passively cooled plate is provided. Similar systems for NEXUS instrument (proposed as a SMEX) and SUMER (flown on SOHO) have had very reasonable properties, but a more detailed solution has yet to be found. A heat rejection mirror will be placed in front of the slit plane to reject the majority of the solar radiation before the slit.

3.3. Strawman Instrument

3.3.1. Optical Design

The EUVS instrument schematic is shown in Figure 3.2. As shown in the schematic, solar radiation is incident on the EUVS off-axis paraboloid primary mirror (ϕ~40cm). The primary mirror focuses an image of the solar disk on the entrance slit and reflective slit jaws. Solar radiation falling outside the instrument field of view is redirected out the front of the instrument with a heat rejection mirror following a similar design used for the SUMER/SOHO and the NEXUS instruments. A slit selection mechanism interchanges and precisely places various slits in the telescope focal plane.

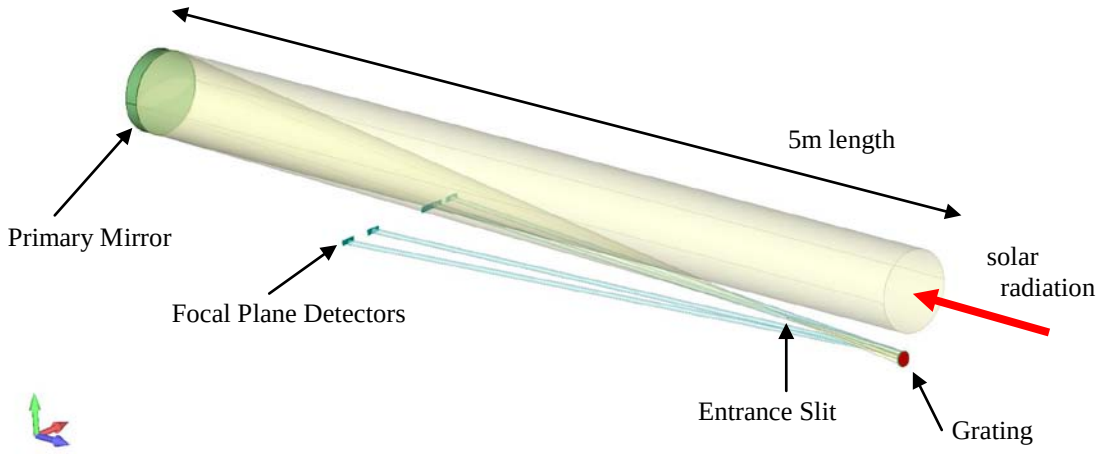

Figure 3.2. EUVS strawman instrument schematic

Solar radiation passing through the slit is reflected and dispersed by the elliptical, variable line space grating onto the various focal plane detectors. The grating may be divided into as many as four separate gratings to cover the various wavelength bands. The figure, ruling, and coating of each grating segment are optimized to meet the requirements of the particular wavelength range. The spectra are recorded by large format, electronic detectors.

3.3.2. Effective Area

Results from a conservative first order effective area calculation for the strawman instrument are given in Figure 3.3. The effective area was calculated using the expected performance of a next-generation, broadband multilayer reflection coating for both mirror and grating. A groove efficiency of 0.40 and detector efficiency of 0.5 were assumed. Each

channel used 0.25 of the mirror total area. The calculated effective area is a factor of >10 higher than previous instrumentation as shown below. Further optimization and refinement of this calculation would likely show considerable improvement. In particular, the use of only two grating sections for the EUV and the FUV ranges will enhance by a factor two the throughput.

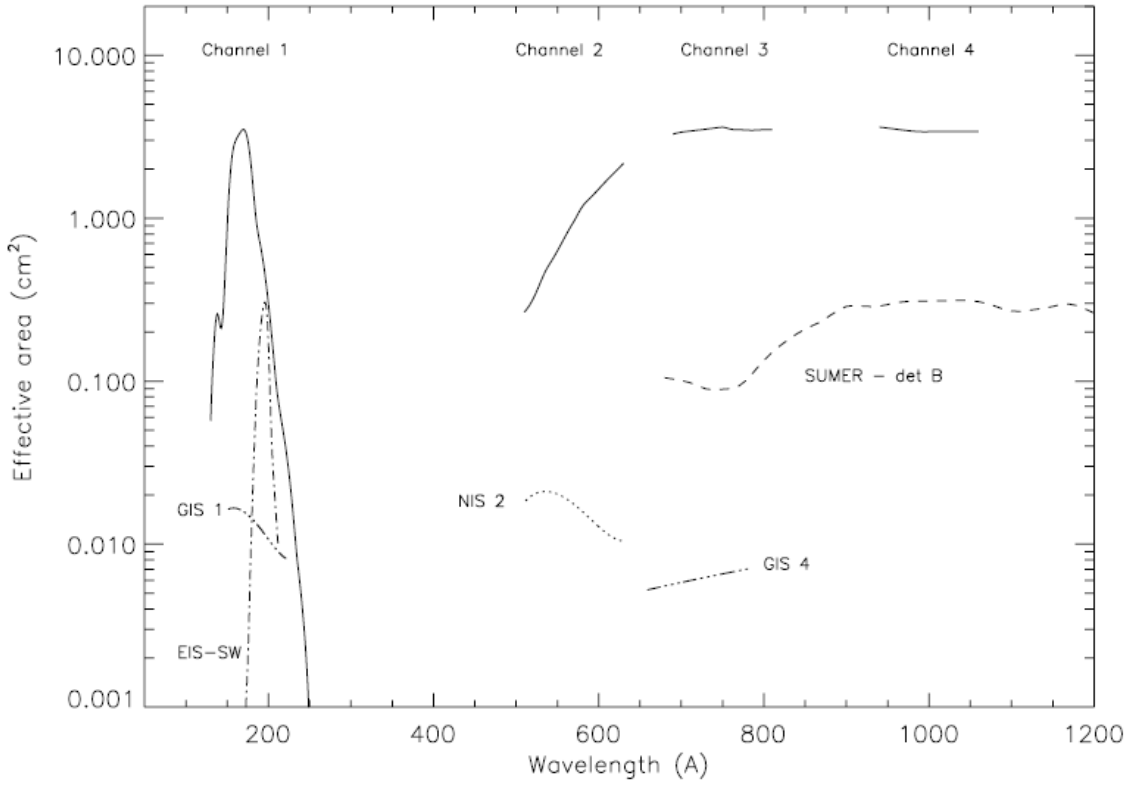

Figure 3.3. Effective area of the EUVS strawman instrument. Previous comparable effective areas for EIS, CDS and SUMER are plotted for comparison.

3.3.3. Selection of wavelength bands

Four spectral bands were chosen as representative for the purpose of developing the strawman design. The bandpasses will be further optimized to meet the specific Solar-C scientific requirements.

3.3.4. Expected count rates and Temperature Coverage

The expected count rates for the emission lines in the four channels have been calculated and are given in Appendix 3-A. The temperature coverage of the bandpasses is superb as shown in Figure 3.4. The total counts in each line for quiet Sun, active regions and flares are given for a spatial sampling of 0.33". Count rates larger than 100 counts/s will allow rastering of quiet-Sun plasmas with 1-s exposure times in the hydrogen H I and the carbon C III lines. Spatial binning and slightly longer integrations allow rapid scanning in a wide variety of fainter lines (C II, He I, O V, Ne VIII, Fe IX, Fe X, etc.) and will yield extraordinary

spectroscopic images of the quiet Sun. Active region count rates of several hundred counts/s with 0.33" spatial resolution enable spectroscopic imaging of active region flows and dynamics. The EUVS line list includes high temperature, well isolated emission lines in flares and active region plasmas.

Figure 3.5 compares the count rates expected for the Solar-C spectrometer with the currently operating SoHO/SUMER and Hinode/EIS and planned IRIS. It is obvious that the Solar-C spectrometer collects much more numbers of photons in 1 sec integration time, even though the spatial resolution is 0.33 arcsec.

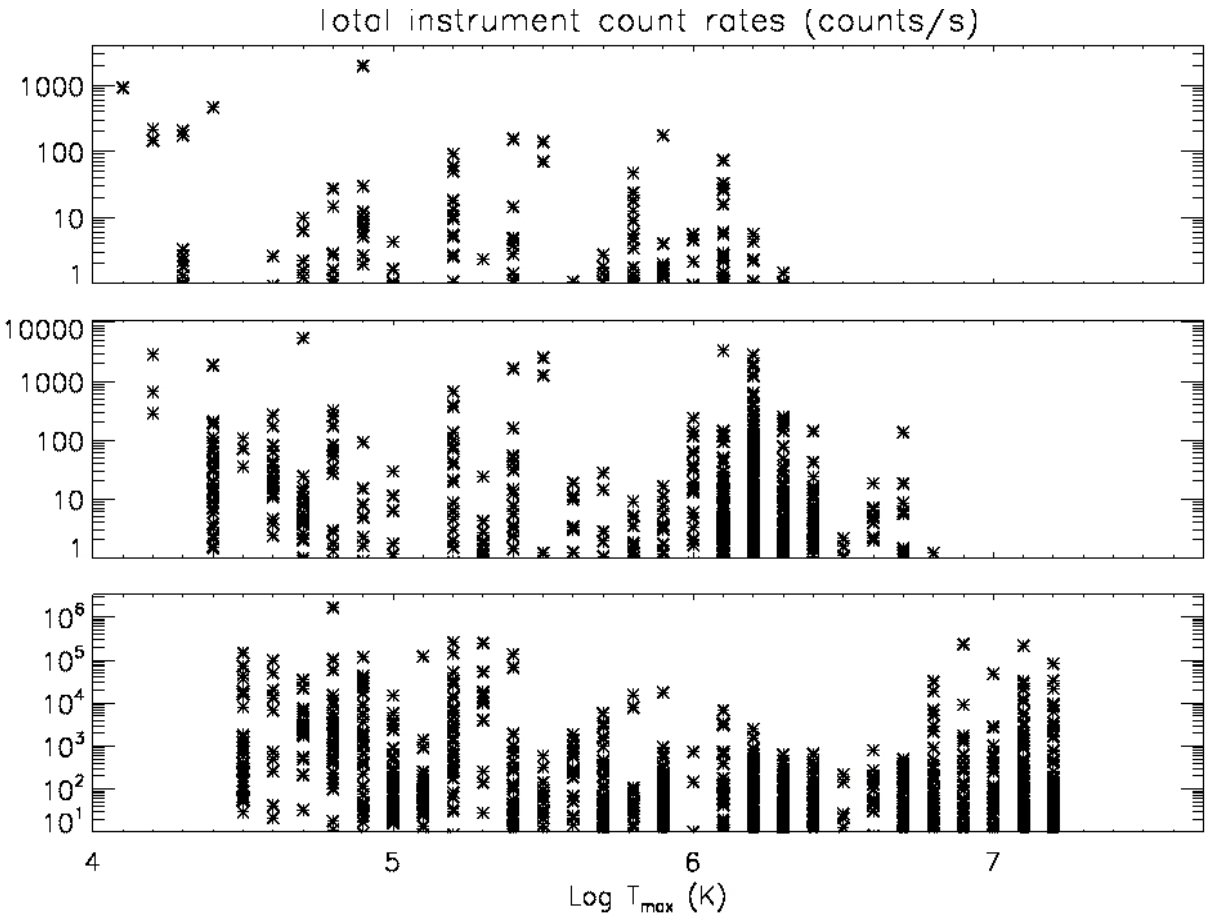

Figure 3.4. Expected Count Rates. The expected count rates are plotted as a function of ionization temperature for a spatial sampling of 0.33". The plots show total counts in each line plotted at their ionization temperature. Each asterisk corresponds to a specific emission line. The top panel corresponds to typical quiet Sun; the middle panel shows typical active region count rates, and the bottom panel shows flare plasma count rates.

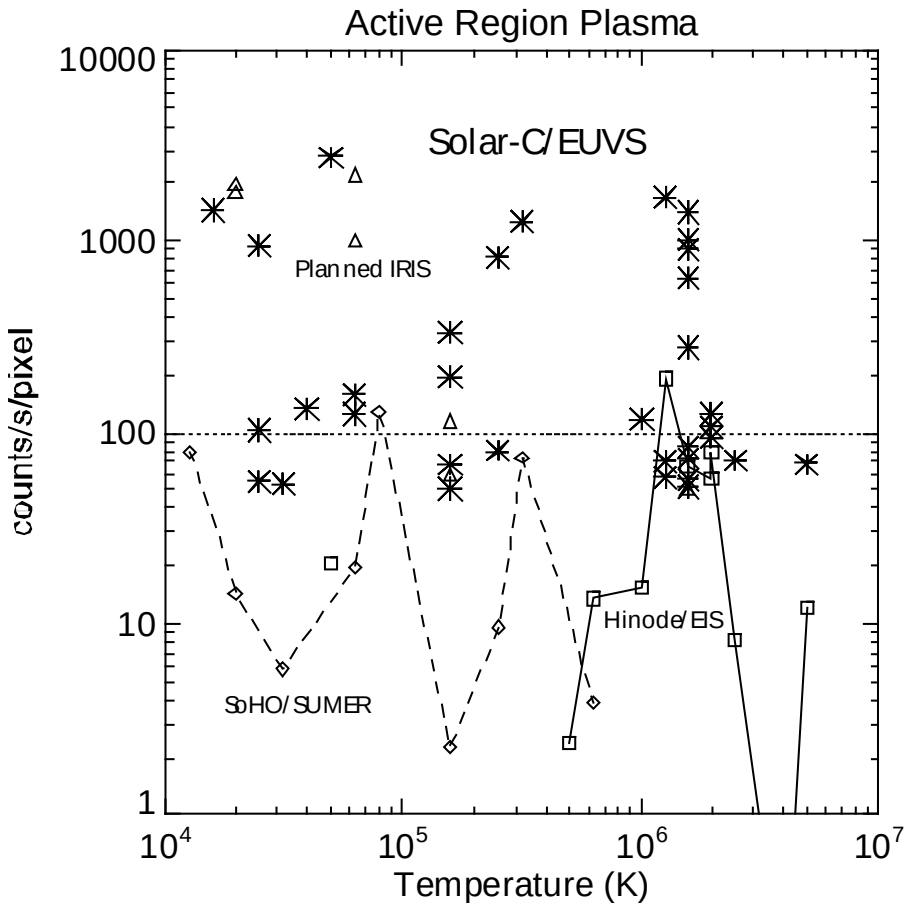

Figure 3.5. Count rates for typical active regions. The Solar-C spectrometer is compared with currently operating SUMER and EIS and planned IRIS. The expected count rates are plotted as a function of ionization temperature for the spatial sampling of each spectometer. Each asterisk corresponds to a specific emission line observed with the Solar-C spectrometer. Triangles, diamonds, and squares are for IRIS, SUMER, and EIS, respectively.

3.3.5. Improvements over previous instrumentation

Critical improvements over previous instrumentation are obtained with this strawman design as follows:

- >18 improvement in spatially resolved area on the solar disk
- >10 improvement in effective area
- complete temperature coverage ($10^4 – 10^7$ K in active regions with $\Delta(\log T) < 0.3$)

A summary table of the EUVS scientific characteristics is given in Table 3.2.

Table 3.2. EUVS scientific summary characteristics.

Plate scale	~0.16"/pixel (sampling comparable to Hinode SOT)
Simultaneous field of view	Slit: 0.16", 0.32", 0.96"; Slot: 10", 40", 200" Slit/slot length: 200" nominal, >300" extended
Maximum raster width	+/- 75" nominal, +/- 200" extended
Wavelength range	four channels (Å):130-250; 510-630; 690-810; 940-1060;
Exposure times	1-5 s with 0.33" spatial sampling 0.1-0.5 s in active regions with 1.0" spatial sampling
Velocity resolution	Doppler (centroid) shift measurement accuracy <3km/s Turbulent velocity (width) <10km/s
Temperature coverage	$10^4 - 10^7$ in active regions with $\Delta(\log T) < 0.3$

3.4. Strawman design details

Further details of the strawman design are given in Table 3.3. Provisions have been made in the strawman design for a slit jaw camera imaging system and a possible closed loop servo-control system using a correlation tracker system and an articulated primary mirror for image stabilization. Solar image rastering is accomplished by tilting the primary mirror.

Table 3.3. EUVS strawman design – nominal performance

Telescope	**Baseline or nominal value**
Type	off-axis paraboloid mirror, single coating optimized for both long and short bands.
optical properties	40cm usable aperture diameter, 400cm focal length, 30cm off-axis distance, <λ/80rms, <0.5nm microroughness, 19.4 microns/arcsecond plate scale.
Mirror blank	Lightweighted premium grade zerodur blank (or equivalent).
Stabilization	<0.03 arcsecond jitter suppression, >5Hz bandwidth possible
Geometric blur	~0.26" at 75" roughly circular field of view, ~0.52" at 150" roughly circular field of view
Slit/slot assembly	**Baseline or nominal value**
General	6 slits/slot positions, front face with reflective coating, >327" length
selected widths	Slits: 0.16", 0.32", 0.96"; Slots: 10", 40", 200"
Slit jaw imaging	**Baseline or nominal value**
General	Projecting a high-quality image of the slit jaws onto a CCD camera. Feeds a CCD camera used for correlation tracker system.
Design char.	field of view: 400" x 400"; plate scale: 0.2"/pixel; CCD format: 2K x 2K.
Filter bandpass	Possible selections include: Ly-α line (121.6 nm), Tmin(160 nm), Mg II line (280 nm), Ca II (393 nm), G-band (430.5 nm), Hα line (656.3 nm), TiO band (705.7 nm).
Correlation tracker system	If implemented is expected to be similar to that used on Hinode/SOT bandwidth (10-30 Hz). Dedicated small-format CCD camera.
Spectrograph characteristics	**Baseline or nominal value**
General	Optimized single reflection EUV spectrograph, elliptical substrate with variable line spacing as required, grating figure and ruling individually optimized for the bandpass/quadrant. Typical blur: <1 pixel over majority of wavelength range for +/- 50" at slit center. Coating selected and optimized for each quadrant. Detector optimized for the bandpass/quadrant
EUV1 bandpass (130-250Å)	detector: 12kx2k mosaic CCD/APS, backside illuminated, 13.5 μm pixel size. stray light rejection: thin film metallic filter with supporting mesh. spatial plate scale: 0.16"/pixel. spectral plate scale: 0.010 Å/pixel, 17.7 km/s-pixel@170Å. Grating: m~4.35, elliptical figure, 4000line/mm VLS ruling, -1 order.

EUV2 bandpass (510-630Å)	detector: 5kx2k CCD/APS, 17 μm pixel size with MCP intensifier with KBr photocathode. stray light rejection: solar-blind intensifier spatial plate scale: 0.20"/pixel. spectral plate scale: 0.026 Å/pixel, 13.7 km/s-pixel@570 Å. grating: m~4.35, elliptical figure, 2000line/mm VLS ruling, +1st order.
EUV3 bandpass (690-810Å)	detector: 5kx2k CCD/APS, 17μm pixel size with MCP intensifier with KBr photocathode. stray light rejection: solar-blind intensifier. spatial plate scale: ~0.20"/pixel spectral plate scale: ~0.025 Å/pixel, 10.0 km/second-pixel @ 750Å. grating: m~4.35, elliptical figure, 2000line/mm VLS ruling, -1st order.
EUV4 bandpass (940-1060Å)	detector: 5kx2k CCD/APS, 17 μm pixel size with MCP intensifier with KBr photocathode. stray light rejection: solar-blind intensifier. spatial plate scale: ~0.20"/pixel. spectral plate scale: ~0.024 Å/pixel,7.2 km/s-pixel@1000 Å. Grating: m~4.35, elliptical figure, 2000line/mm VLS ruling, +1st order.

3.5. Further optimization for better instrument

Considerable optimization activities remain for the spectrograph instrument. Science goals and associated measurement requirements need further definition. The trades relating to instrument wavelength ranges need further definition. The number of channels drives instrument complexity. The wavelength ranges should be placed more conveniently on various detectors. The size and f# of the primary mirror strongly drive the instrument mass and envelope. The primary mirror size also drives the design of the articulated mirror mechanism and associated requirements. The optical design may be further optimized for the wavelength ranges and detectors selected. The coatings of the mirror and gratings could also be optimized for the particular application.

Appendix 3-A. EUVS count rates for the brightest lines

Count rates were calculated for the EUVS instrument using the CHIANTI spectral code for the quiet Sun, active region and flare plasmas. The counts listed are for the total emission line in a 0.33" spatial bin. The emission lines are sorted by channel and ionization temperature. The ion and associated ionization temperature are included for reference. For the quiet Sun, all lines with a total count rate of >10 counts/s are included. For active regions, emission lines with a total count/s of >50 were tabulated. For flare plasmas, those emission lines with count rates >10000 counts/s are included. Many valuable faint diagnostic lines have not been tabulated.

QUIET SUN INTENSITIES

Ion	Wvl.(A)	Tmax	Count/s
Fe IX	171.073	5.90	86.9
Fe X	174.531	6.10	36.4
Fe X	177.240	6.10	16.4
Fe XI	180.408	6.10	14.1
He I	584.335	4.40	230.7
O V	629.732	5.40	76.5
Mg X	609.794	6.10	13.0
O III	703.854	4.90	14.7
N IV	765.147	5.20	29.5
O IV	787.710	5.20	24.9
O IV	790.199	5.20	45.1
Ne VIII	770.410	5.80	23.5
Ne VIII	780.325	5.80	11.9
H I	949.745	4.20	71.2
H I	972.538	4.20	107.3
H I	1025.724	4.10	453.1
C II	1036.339	4.30	87.5
C II	1037.020	4.30	102.2
C III	977.020	4.90	98.9
N III	991.577	4.80	13.6
O VI	1031.914	5.50	69.6
O VI	1037.615	5.50	34.9

The lines counted in this table have all a count rate greater than 10.0000

ACTIVE REGION INTENSITIES

Ion	Wvl.(A)	Tmax	Count/s
Fe VIII	167.486	6.00	71.0
Fe VIII	168.173	6.00	118.0
Fe VIII	168.544	6.00	58.7
Fe IX *	168.647	6.10	59.8
Fe IX	171.073	6.10	1671.6
Ni XI	148.374	6.20	56.3
Ni XII	152.154	6.20	73.4
Ni XII	154.162	6.20	50.4
Ni XIII	157.729	6.30	125.3
Ni XIII	164.150	6.30	90.8
Ni XIV	170.500	6.30	72.2
Ni XIV	171.370	6.30	108.2
Fe X	174.531	6.20	1408.2
Fe X	175.263	6.20	153.2
Ni XV	176.741	6.40	71.2
Fe X	177.240	6.20	637.8
Fe XI	178.060	6.20	57.7
Fe XI	180.408	6.20	900.6
Fe X	180.441	6.20	62.9
Fe XI	181.137	6.20	59.0
Fe XI	182.169	6.20	128.8
Fe X	184.537	6.20	110.7
Fe XII	186.887	6.20	91.5
Fe XI	188.232	6.20	195.6
Fe XI	188.299	6.20	71.0
Fe XII	192.394	6.20	108.4
Fe XII	193.509	6.20	212.0
Fe XII	195.119	6.20	277.7
Fe XIII	202.044	6.20	85.1
He I	584.335	4.40	936.4
O IV	554.513	5.20	50.4
O V	629.732	5.40	822.3
Si XII	520.666	6.30	94.8
Si XI	580.920	6.20	51.6
Mg X	609.794	6.20	1010.1
Mg X	624.943	6.20	613.9
O III	703.854	4.80	125.8
O II	718.506	4.60	134.1
O II	718.568	4.60	86.7
O V	760.446	5.40	80.1
N IV	765.147	5.20	195.3
S V	786.470	5.20	67.6
O IV	787.710	5.20	184.4
O IV	790.199	5.20	334.0
Mg IX	706.036	6.10	70.6
Ne VIII	770.410	6.20	636.5
Ne VIII	780.325	6.20	319.7
H I	949.745	4.20	143.0
H I	972.538	4.20	336.1
H I	1025.724	4.20	1441.1
C II	1036.339	4.40	95.0
C II	1037.020	4.40	103.3
S II	1045.765	4.40	54.8

C III	977.020	4.70	2728.3
N III	989.799	4.80	86.6
N III	991.577	4.80	159.3
C II	1010.373	4.50	53.1
O VI	1031.914	5.50	1258.7
O VI	1037.615	5.50	631.0
Si VIII	944.467	6.10	57.7
Fe XVIII	974.860	6.70	68.3

The lines counted in this table have all a count rate greater than 50.0000

FLARE INTENSITIES

Ion	Wvl.(A)	Tmax	Count/s
Fe XXIII	132.906	7.20	16711.9
Fe XXII	135.791	7.10	10684.5
Fe XXII	156.019	7.20	10742.9
Fe XXIV	192.029	7.20	41466.6
He I	584.335	4.50	22806.8
O III	599.590	4.90	21647.0
O IV	554.513	5.20	16856.3
O IV	609.829	5.20	13597.1
O V	629.732	5.30	123868.6
Mg X	609.794	6.80	15972.9
Fe XX	567.867	7.10	14098.6
Fe XIX	592.236	7.00	24262.3
O III	702.337	4.90	15646.4
O III	702.838	4.90	14272.3
O III	702.896	4.90	12071.4
O III	702.900	4.90	19085.9
O III	703.851	4.90	19602.9
O III	703.854	4.90	58808.9
O II	718.506	4.70	17162.6
O II	718.568	4.70	11081.7
N IV	765.147	5.10	61374.2
O V	760.446	5.30	26905.2
S V	786.470	5.20	26186.6
O IV	787.710	5.20	71908.2
O IV	790.112	5.20	13861.8
O IV	790.199	5.20	128603.8
Fe XX	721.559	7.10	108802.5
Fe XXI	786.162	7.10	16011.5
H I	972.538	4.50	18466.2
C III	977.020	4.80	834613.1
N III	989.799	4.80	29670.6
N III	991.577	4.80	52456.0
C II	1010.373	4.60	10053.1
H I	1025.724	4.50	72905.9
H I	1025.725	4.50	36616.4
C II	1036.339	4.60	24846.7
C II	1037.020	4.60	49448.2
O VI	1031.914	5.40	67592.8
O VI	1037.615	5.40	33837.3
Fe XVIII	974.860	6.90	116048.3

The lines counted in this table have all a count rate greater than 10000.0